A Compact 16-Module Camera Using 64-Pixel CsI(Tl)/Si PIN Photodiode Imaging Modules

W.-S. Choong, *Member, IEEE*, G. J. Gruber, W. W. Moses, *Senior Member, IEEE*, S. E. Derenzo, *Fellow, IEEE*, S. E. Holland, *Member, IEEE*, M. Pedrali-Noy, *Member, IEEE*, B. Krieger, *Member, IEEE*, E. Mandelli, *Member, IEEE*, G. Meddeler, *Member, IEEE*, N. W. Wang, and E. K. Witt

***Abstract*—We present a compact, configurable scintillation camera employing a maximum of 16 individual 64-pixel imaging modules resulting in a 1024-pixel camera covering an area of 9.6 cm x 9.6 cm. The 64-pixel imaging module consists of optically isolated 3 mm x 3 mm x 5 mm CsI(Tl) crystals coupled to a custom array of Si PIN photodiodes read out by a custom integrated circuit (IC). Each imaging module plugs into a readout motherboard that controls the modules and interfaces with a data acquisition card inside a computer. For a given event, the motherboard employs a custom winner-take-all (WTA) IC to identify the module with the largest analog output and to enable the output address bits of the corresponding module's readout IC. These address bits identify the "winner" pixel within the "winner" module. The peak of the largest analog signal is found and held using a peak detect circuit, after which it is acquired by an ADC on the data acquisition card. The camera is currently operated with 4 imaging modules in order to characterize its performance. At room temperature, the camera demonstrates an average energy resolution of 13.4% FWHM for the 140 keV emissions of ^{99m}Tc. The system spatial resolution is measured using a capillary tube with an inner diameter of 0.7 mm and located 10 cm from the face of the collimator. Images of the line source in air exhibit average system spatial resolutions of 8.7 mm FHWM and 11.2 mm FWHM when using an all-purpose and a high-sensitivity parallel hexagonal holes collimator, respectively. These values do not change significantly when an acrylic scattering block is placed between the line source and the camera.**

***Index Terms*—compact gamma camera, photodiode array, pixellated scintillator, low-noise integrated circuit readout, scintimammography.**

I. Introduction

SINCE its invention in 1958, the Anger camera has proven to be an important instrument in nuclear medicine imaging. However, Anger cameras are not optimized for the task of breast or axillary node imaging because of their bulky size and significant dead space around the periphery of the camera. The large camera size makes access to the breasts and axillae difficult, resulting in a long imaging distance which decreases spatial resolution and detection sensitivity. These limitations can be lessened through compact camera design. Other small organ imaging applications, small animal imaging applications, and applications involving surgical probes would all also benefit from compact gamma cameras.

There are three major design approaches to the development of compact gamma cameras: (1) discrete scintillator/photodiode cameras wherein the gamma rays interact in an array of optically isolated scintillation crystals coupled 1-to-1 to an array of solid-state photodetectors [1]-[5]; (2) solid-state cameras where the gamma rays interact directly with a pixellated solid-state detector such as CdZnTe [6]-[8]; and (3) position-sensitive photomultiplier tube (PSPMT) cameras where the gamma rays interact in one or more scintillation crystals which are subsequently read out by a single PSPMT [9]-[14]. Each approach has its own unique advantages and challenges. However, one of the common technological challenges shared by these approaches is to achieve a system that matches and/or improves Anger camera performance, particularly with regard to energy resolution, reliability, and cost. In this paper, we present a 16-module compact camera using 64-pixel imaging modules consisting of discrete CsI(Tl) crystals coupled to custom low-noise Si PIN (p-layer, intrinsic layer, n-layer) photodiodes which are read out by custom IC. This approach represents a complete modular design that can be used to realize a variety of compact gamma camera configurations.

II. 64-Pixel Imaging Module

The 64-pixel imaging module is a culmination of previous work from a 12-pixel prototype module [2] to the current 64-pixel module [15]. Fig. 1 shows a photograph of the complete module. The design requires making the module as compact as possible as well as modular enough to tile individual modules together to form a larger imaging area with minimal dead area between modules.

The two critical components that make this possible are the custom low-noise Si PIN photodiodes [16] and the custom

Manuscript received Nov 25, 2001. This work was supported in part by the U.S. Department of the Army under grant No. DAMD17-98-1-8302, in part by the U.S. Department of Energy under contract No. DE-AC03-76SF00098, in part by Public Health Service Grants Nos P01-HL25840 and R01-CA67911, in part by the Fannie and John Hertz Foundation, and in part by the University of California at Berkeley.

W.-S. Choong, G. J. Gruber, W. W. Moses, S. E. Derenzo, S. E. Holland, M. Pedrali-Noy, B. Krieger, E. Mandelli, G. Meddeler, N. W. Wang are with the Lawrence Berkeley National Laboratory, Berkeley, CA 94720 USA (telephone: 510-486-6757, e-mail: wschoong@lbl.gov).

E. K. Witt is with Capintec, Inc, Ramsey, NJ 07446 USA (telephone: 201-825-9500, e-mail: ewitt@capintec.com).

readout IC [15]. The former replaces the bulky and expensive PMTs used in Anger cameras, while the latter provides processing for the large pixel density (~ 1 pixel / 10 mm^2).

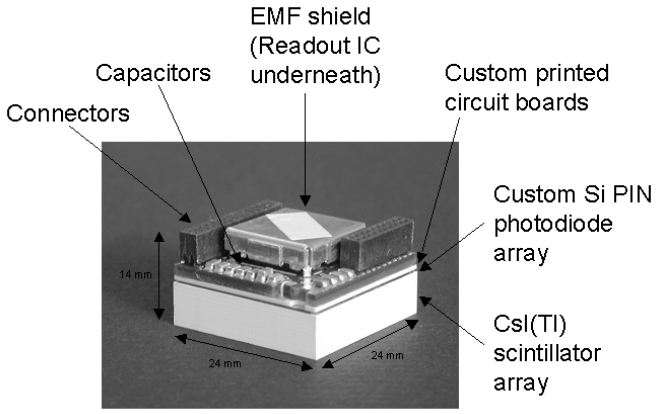

Fig. 1. A complete 64-pixel CsI(Tl) scintillator/Si PIN photodiode imaging module. Two separate custom printed circuit boards are employed to provide all necessary connections to the both the photodiode array and the readout IC. The module has a transverse size of 24 mm x 24 mm and a height of 14 mm.

A. Custom Low-Noise Photodiode Arrays

The low-noise photodiode arrays employed in the imaging modules are the first reliable devices with sufficiently low room temperature leakage current to provide adequate SNR for the application under consideration [16].

The photodiode arrays are made on 300 μm thick, high-resistivity, n-type silicon. The patterned side of the photodiode array consists of 64 3 mm x 3 mm pixels. A series of guard rings run around the perimeter of the patterned side to sink surface leakage current. Since the array is designed to maintain a 3 mm pitch between pixels when butted up against other arrays, the edge and corner pixels have smaller area (30% and 50% smaller, respectively) than the inner pixels. The backside of the array is unpatterned and a 67.9 nm thick anti-reflective layer of indium-tin-oxide (ITO) is deposited on it to optimize transmission of the 540 nm scintillation photons of CsI(Tl).

The pixels demonstrate a capacitance of about 3 pF and an average leakage current of 28 ± 7 pA at room temperature and 50 V bias. The guard rings exhibit an average current of 1.7 ± 0.4 nA.

B. Custom Readout IC

The readout IC is described in detail in [17]. It is a mixed analog-digital design fabricated in CMOS (HP 0.5 μm 3.3 V technology) and covering an area of 4.5 mm x 4.8 mm. Its front-end is an array of 64 analog input channels consisting of charge-sensitive preamplifiers and shaper amplifiers. It is then followed by a "Winner Take All" (WTA) circuitry which reduces the 64 amplified, shaped signals to a single analog signal with the largest amplitude plus 6 digital bits that identify the winning channel. The WTA circuitry is based on a 16-channel WTA IC described in [18].

III. 16-Module Camera Design

The basic design and the system level diagram for the 16-module compact camera are presented in Fig. 2. A maximum of 16 individual 64-pixel imaging modules can be plugged into a readout motherboard that controls the modules and interfaces with a computer. The result is a 1024-pixel camera covering an area of 9.6 cm x 9.6 cm. The motherboard is designed such that its electronics extend beyond the imaging area in only one direction, thus preserving the camera's ability to gain close access to the breasts and axillary nodes.

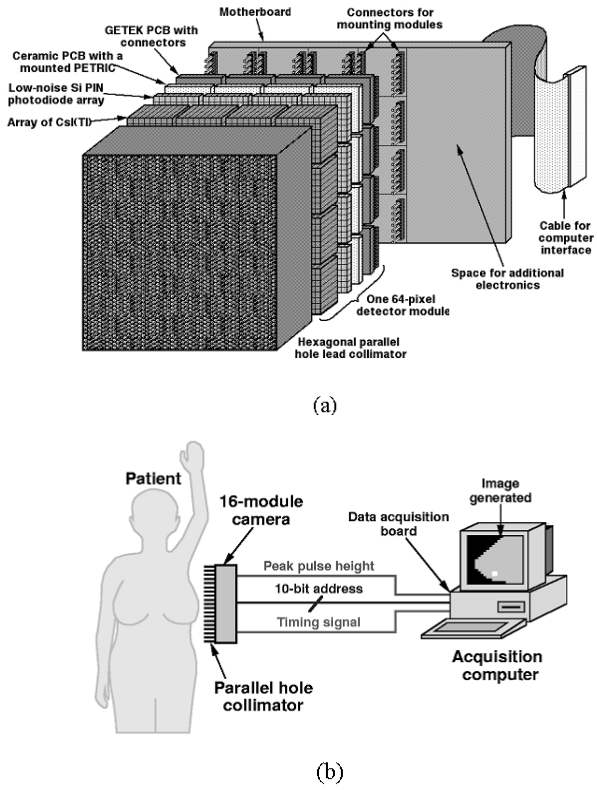

Fig. 2. System level diagram for the 16-module camera showing: (a) the design of the camera constructed from 16 individual 64-pixel modules: and (b) how the camera is to be employed.

A patient or other radionuclide distribution is imaged with the camera while employing a parallel hexagonal hole collimator to provide directional information. For a given event, the camera produces the following outputs: (1) the peak voltage of the analog shaped pulse, which was generated by the imaging module and readout motherboard in response to a gamma ray interaction; (2) the 10-bit digital address indicating the pixel of interaction; and (3) a timing strobe which signals the computer to acquire (via a data acquisition card) both the current pulse height voltage and the digital address bits. Energy discrimination and any other data processing take place within the data acquisition software. The information for the event is then incorporated into the image data.

A. Readout Motherboard

The readout motherboard is separated into two sections as shown in Fig. 3: (1) the imaging section; and (2) the

electronic section. The imaging section lies on one side of the motherboard where the individual imaging modules connect to mating connectors. The electronic section lies on the other side, preserving the camera's ability to gain close access to the breasts and axillary nodes.

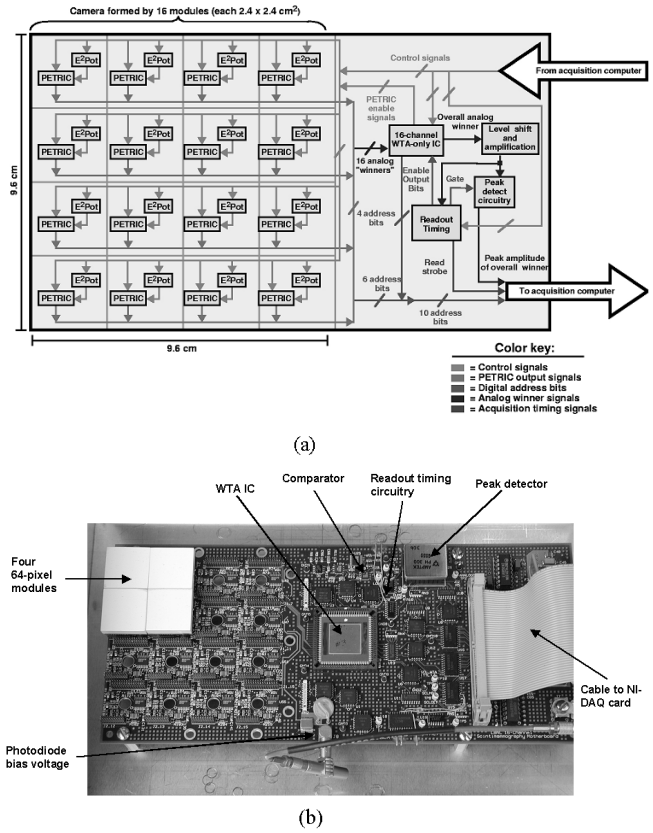

Fig 3. (a) Block diagram of the 16-module readout motherboard used to integrate 16 64-pixel imaging modules. (b) Photograph of the readout motherboard with 4 imaging modules connected to it.

The power, ground, and control signals (both analog and digital) are provided to the readout ICs on the modules via the mating connectors. The 16 different readout ICs on the modules are distinguished from each other by hardwired 4-bit addresses. Communications with the individual readout ICs is implemented using a serial data and serial clock protocol with ECL logic. In addition to the digital protocol, the readout IC must be provided with 4 bias currents. Module-by-module adjustments of these currents are achieved by employing non-volatile, digital potentiometers (E^2Pot IC, X9241, from Xicor, Inc., Milpitas, CA). Each E^2Pot IC contains 4 separate potentiometers whose resistance can be adjusted using the serial protocol.

A 16-channel WTA IC [18] is employed to multiplex the "winner" analog output signals from the 16 imaging modules to the data acquisition card along with a 4-bit digital address denoting the module from which the winner was generated. In addition, the WTA IC controls the readout IC digital output enable signals. These output enable signals determine whether a given readout IC can drive its digital output lines (6 address bits plus 2 error checking bits) or leave them in a high-Z state. This feature is important is two respects. First, this means that the 8 digital output lines from each readout IC can be tied together, and the lines will be driven only by the readout IC producing the winning signal. Second, the moment the output enable signals are active, digital noise is coupled into the preamplifier of the readout IC, resulting in decreased SNR. Therefore, the digital output lines are enabled only after the winner analog signal has been latched into the ADC on the data acquisition card. Soon thereafter the output enable signal of the winner readout IC is made active and the digital output lines are latched into the data acquisition card. Ultimately, an event is characterized by the analog winner signal's peak voltage and the 10-bit digital address of the winning pixel.

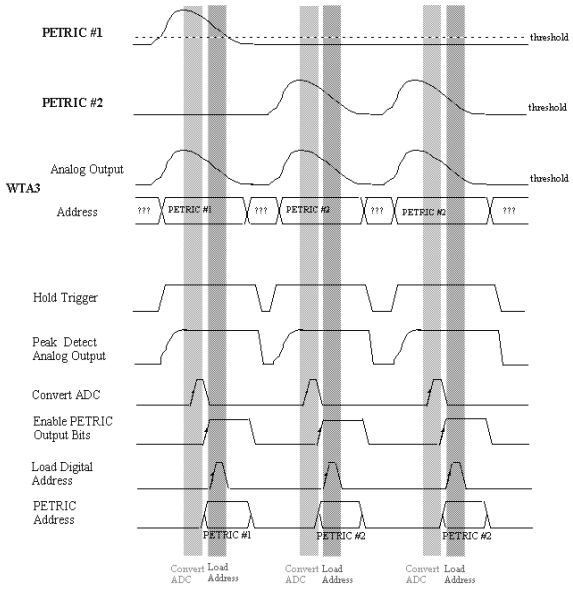

Fig. 4. Timing diagram for data acquisition signals in the 16-module camera. A simple case involving two readout ICs being serviced by the 16-module WTA IC is presented. The readout chain begins with the winner analog output crossing the threshold and lasts until the data for the event has been successfully collected.

A simple threshold discriminator is used to eliminate low-voltage noise signals. Once the 16-channel WTA analog output signal crosses the threshold, the motherboard begins a readout chain to collect the data for the event. Fig. 4 summarizes the timing of the different signals in the readout hierarchy. The processing time for an event is controlled by a one-shot with adjustment through an E^2Pot. The analog output signal of the readout IC is adjusted to have a peaking time of about 6.5 μs (appropriate for CsI(Tl) scintillation). The processing time is set at 40 μs, the time it takes the analog output signal to return to baseline. During this time, additional analog output signals are ignored. A peak detect IC (PH300, Amptek, Inc., Bedford, MA) is employed to hold the peak value of the signal until it is latched into the ADC. After the peak value of the signal has been digitized, the output enable of the readout IC producing the winner analog output is made active, thus driving the digital output lines which are subsequently read into the data acquisition card. The motherboard will return to its default state after each

processing time because the timing circuitry is implemented to avoid any "lock-up" whereby after it fails to finish processing the signal in question, it is further unable to process any additional signals. The processing time determines the camera dead time. However, the maximum event rate remains adequately high because the dead time is non-paralyzable. For example, a true event rate of 10 kHz would give an observed event rate of about 7.1 kHz (a loss of about 29 %). A shorter processing time can be used to increase the maximum rate. In theory, processing times as short as 10 μs can be used, that is the time it takes to latch both the analog output signal and the digital output lines. In practice, rates are low enough that we observe no dead time effects.

The readout IC and the 16-channel WTA IC share a serial data bus line using ECL logic. The E^2Pots use a separate serial data bus line because they employ TTL logic. Further, the readout ICs, the 16-channel WTA IC, and the E^2Pots use separate serial clock lines to prevent commands on the serial data line that are intended for one type of chip from being latched into the chip of the other type with the same 4-bit chip address. Communication to and from a computer is implemented by means of a general purpose analog, digital, and timing I/O board (DAQCard-1200, National Instruments, Austin, TX) controlled by a PC laptop system running LabVIEW.

B. Collimator Design

The classic tradeoff between collimator spatial resolution and sensitivity is an important consideration in the design of the collimator. Traditional scintillation cameras use hexagonal hole collimators. The advantages of hexagonal hole collimators are that they are more readily available from industry and have a more symmetric septal penetration pattern. However, square holes can be matched 1-to-1 (or even 4-to-1) to square detector pixels and thus may provide a superior system point spread response with minimal dependence on source position by eliminating the aliasing due to geometric mismatch between hexagonal collimator holes and square detector pixels.

Previous simulation suggests that this aliasing problem is small for hexagonal hole collimators if the hole size is less than about half the pixel size [2]. In addition, simulation suggests that observed tumor FWHM shows little difference between hexagonal hole and square hole collimators, while tumor SNR is highly dependent on collimator sensitivity (but again, not hole shape) [19]. Collimators with high sensitivities of 8000 to 16,000 counts/mCi/sec yield significantly better tumor SNR values than do high resolution collimators with 4000 counts/mCi/sec. Further, those higher collimator sensitivities only slightly increase observed tumor FHWM at short imaging distance (less than 7 cm).

Based on the simulation results [2], [19], we have designed and acquired three collimators (Nuclear Fields, Inc., Des Plaines, IL) for use with the 16-module camera. All three collimators are microcast from lead, cover an area 10 cm x 10 cm, and employ parallel hexagonal holes with a diameter of 1.5 mm and a septal thickness of 0.25 mm. The only difference between the collimators is the channel length, which determines the sensitivity and spatial resolution.

Table I provides the design specifications for the three collimators. The collimators have been designed with high sensitivities (ranging from 8000 to 26,000 counts/mCi/sec) in order to improve the SNR of any high-uptake objects in the resulting planar images. The spatial resolutions of 6.1 mm to 9.8 mm FWHM at 6 cm imaging distance still provide for the possibility of detecting tumors less than 1 cm in diameter, especially if the SNR in the planar image is reasonably high.

TABLE I
THREE COLLIMATOR DESIGNS FOR USE WITH THE 16-MODULE CAMERA

	All-purpose	High-sensitivity	Ultra high-sensitivity
Channel length (mm)	23.5	16.5	13.0
Sensitivity (counts/mCi/sec)	8020	16,200	26,200
Spatial resolution @ 6 cm (mm)	6.1	8.0	9.8
Septal penetration (%)	0.6	2.6	5.6

IV. CAMERA PERFORMANCE

The compact 16-module camera has initially been operated with 4 imaging modules. We have assembled over 16 modules for use with the camera (most of them without the CsI(Tl) arrays glued on to the backside of the photodiode arrays). Unfortunately, the electronic noise from most of the modules is not acceptable due to mishandling of the photodiode arrays by the vendor that attached them to the printed circuit board. We are working closely with the vendor to refine their assembly procedures so that the quality of future modules is good.

A. Intrinsic Energy Resolution

Pulse height spectra are collected for each pixel by exciting the modules with 140 keV emissions from ^{99m}Tc. Fig. 5 shows typical pulse height spectra for corner, edge and inner channels from a single module. The smaller corner and edge pixels have significant impact on the energy resolution (the light collection efficiency for these pixels is less, resulting in lower SNR). The average energy resolution for the camera is 13.4% FWHM. Not all modules have similar energy resolution because the overall electronic noise varies from one module to the other. Fig. 6 shows the distribution of the energy resolution for a module with high SNR, while Fig. 7 shows distribution for a module with low SNR.

Module noise performance is characterized by measuring noise as a function of the shaper peaking time. Equivalent noise charge (ENC) is calculated by calibrating the signal with an ^{55}Fe source before the CsI(Tl) arrays are glued on. Fig. 8 shows a module with good electronic noise performance, while Fig. 9 shows a module with significantly higher electronic noise. Both of these modules are used with the camera. When unloaded, the electronic noise approaches

the 1/f floor limit as the high peaking time increases. The noise obtains a parallel noise contribution with the addition of a photodiode load, causing the noise to increase with peaking time. The corner and edge pixels exhibit lower noise because of lower capacitance and leakage current. For certain modules, the electronic noise is higher due to mishandling of the photodiode array, resulting in an increase in leakage current and 1/f noise.

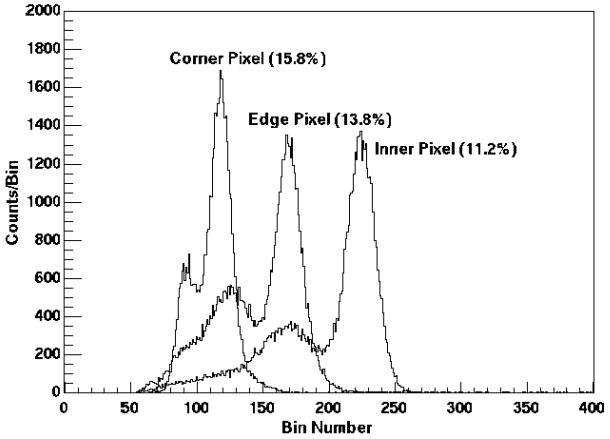

Fig. 5. Room temperature pulse height spectra for typical corner, edge and inner pixels excited by 140 keV emissions of ^{99m}Tc. The numbers in parentheses are the corresponding energy resolution.

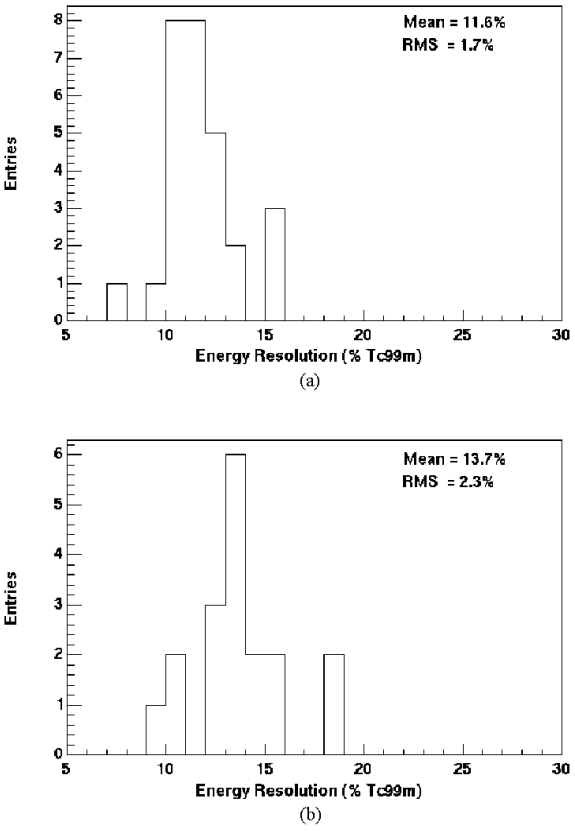

Fig. 6. Histograms of energy resolution (FWHM) demonstrated by (a) inner and (b) edge pixels for a high SNR module.

Another major noise contribution is the CsI(Tl) light collection inhomogeneity. We have obtained CsI(Tl) arrays from three different manufacturers (Hilger, Photopeak, and Bicron). Each pixel is separated by 0.2 mm thick reflector material. The performance of the arrays is measured by cutting individual crystals from each manufacturer, coupling them to a PMT, exciting them with 511 keV gammas, and measuring their output with an Ortec gated integrator amplifier. The results are shown in Fig. 10.

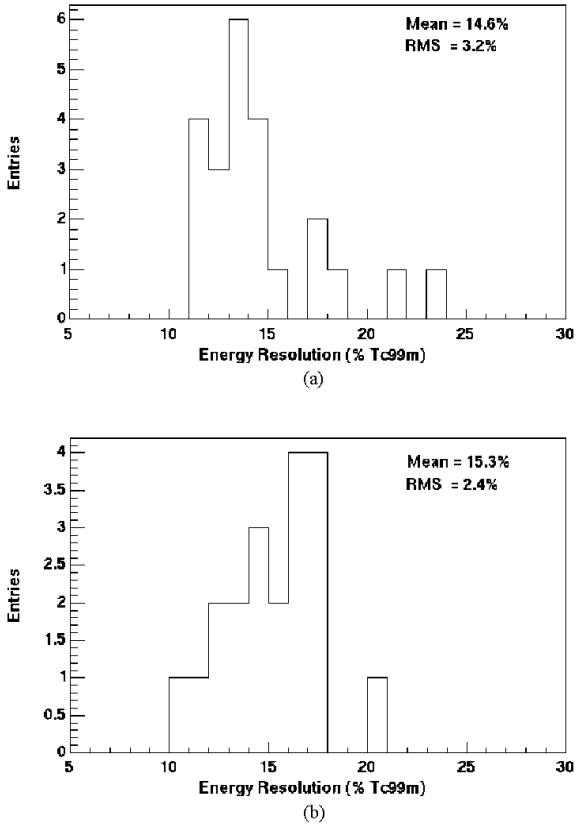

Fig. 7. Histograms of energy resolution (FWHM) demonstrated by (a) inner and (b) edge pixels for a low SNR module.

The results indicate that the Bicron arrays have the highest light output and best energy resolution. The second batch from Hilger obtained about two years ago shows significant degradation in their performance compared to an earlier batch obtained over 4 years ago. We have been informed by representatives from Hilger that their process has changed since the production of the first batch, and they are looking into methods of regaining the performance in the earlier batch. The 4 imaging modules on the camera have the Photopeak arrays on it.

In an attempt to understand the cause of the performance difference among the different crystals, we removed the reflector material from each of the manufacturer arrays, rewrapped them in plumber's Teflon tape, and repeated the measurement. The results show that the crystals from all three manufacturers have similar performance. This suggests that the performance difference comes from the characteristics of

the reflector material, and/or the coupling of the reflector material to the surface of the crystals.

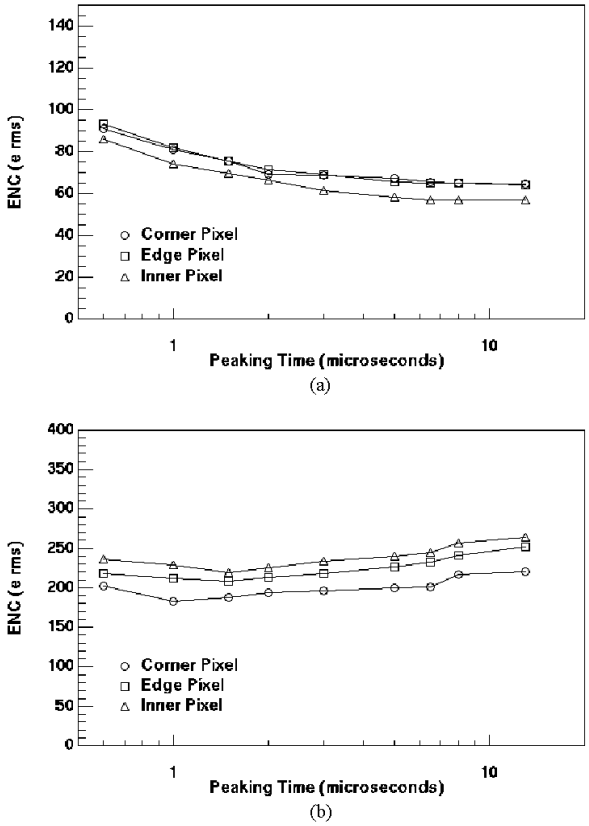

Fig. 8. ENC as a function of peaking time for a low electronic noise module (a) without and (b) with the photodiode attached.

B. *Intrinsic Spatial Resolution*

The intrinsic spatial resolution of the camera has been measured by scanning a collimated ^{57}Co beam across the face of a imaging module [15]. The result is consistent with the crystal size of 3 mm.

C. *System Spatial Resolution*

The system resolution is measured with a line source made from glass capillary tube filled with ^{99m}Tc as specified by the National Electrical and Manufacturers Association (NEMA) standards of measurement [20]. The capillary tube has a length of 7.5 cm, an inner diameter of 0.7 mm, and is placed 10 cm from the face of the collimator. Fig. 9 shows the images of the line source taken in the X and Y direction, with the all-purpose and then the high-sensitivity collimator, with an acrylic scattering block placed between the source and the face of collimator.

The FWHM of the spatial resolution is calculated by fitting slices of the line source images with a Gaussian function plus a linear background. The FWHM in pixels is then multiplied by the pixel size (3 mm) to yield the FWHM in mm. Table II summarizes the results of the measurement. The spatial resolution exhibits little dependence on whether or not the scattering blocks is used. On the other hand, the spatial resolution increases significantly with the high-sensitivity collimator because the collimator spatial resolution dominates at long imaging distance (greater than 7 cm).

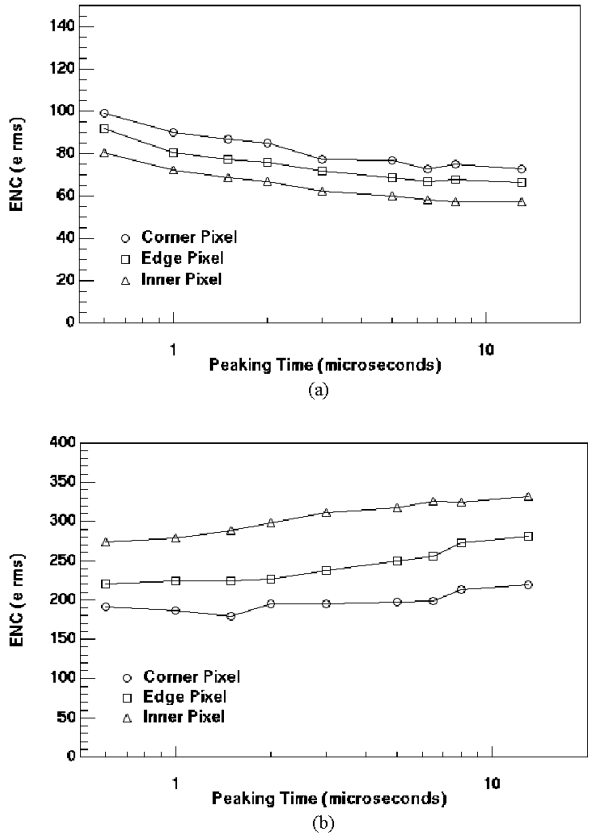

Fig. 9. ENC as a function of peaking time for a high electronic noise module (a) without and (b) with the photodiode attached.

V. Conclusions And Future Work

A compact 16-module camera using 64-pixel imaging module has been implemented. The key and innovative advances in the development of the 64-pixel module are: (1) the low leakage current Si PIN photodiode arrays, and (2) the readout IC that allows efficient readout of many channels. In addition, at the heart of the 16-module camera is the 16-channel WTA IC, which multiplexes the largest analog output signals from the 16 modules on the camera to a single winner analog output. An obvious drawback of this multiplexing scheme is a decrease in the maximum event rate in the camera. However, the maximum event rate remains adequately high because the collimator significantly reduces the gamma flux and the dead time can be made as short as 10 μs per event (the time it takes to successfully latch both the analog output signal and the digital output lines).

The camera operated with 4 imaging module demonstrates an average energy resolution of 13.4% FWHM for 140 keV gammas. Corner and edge pixels have a slightly higher energy resolution because their smaller pixel size results in lower light collection efficiency. Monte Carlo simulation [19] suggests that improving energy resolution much below 15% does not significantly improve breast tumor imaging as the main background contribution in planar image is not scattered

but un-scattered emissions from non-specific uptake in normal breast tissue.

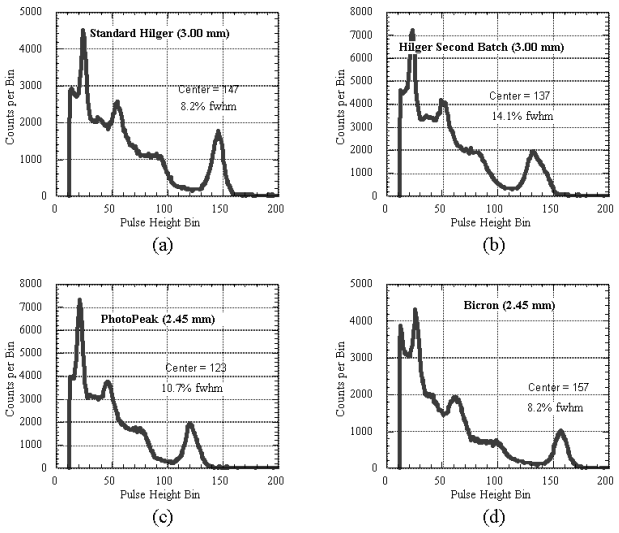

Fig. 10. Pulse height spectra of CsI(Tl) array from three different manufacturers.

The system spatial resolution of the camera demonstrates the possibility of detecting tumors less than 1 cm in diameter with the all-purpose or high-sensitivity collimator, especially at short imaging distance.

The future direction for this work includes constructing a multi-module camera using a smaller pixel size (2.4 mm x 2. 4 mm) photodiode array. In addition, a new WTA IC with 32 input channels and peak detect circuitry has been designed and fabricated to be used in future compact cameras.

VI. Acknowledgment

We would like to thank Dr. T. F. Budinger for his advice regarding this research. We further thank C. S. Tindall for processing the photodiode arrays, M. H. Ho for his contributions in the lab, and G. J. Zizka for his extensive wirebonding efforts.

This work was supported in part by the U.S. Department of the Army under grant No. DAMD17-98-1-8302, in part by the Director, Office of Science, Office of Biological and Environmental Research, Medical Science Division of the U.S. Department of Energy under Contract No. DE-AC03-76SF00098, in part by the Laboratory Technology Research Division SC-32, (formerly called ERLTT), Office of Science, U.S. Department of Energy under a CRADA (Cooperative Research and Development Agreement) between Lawrence Berkeley National Laboratory and Capintec, Inc., Ramsey, NJ under US DOE Contract DE-AC03-76SF00098, and in part by the National Institutes of Health, National Cancer Institute under grant No. R01-CA67911, and National Institutes of Health, National Heart, Lung, and Blood Institute under grant No. P01-HL25840.

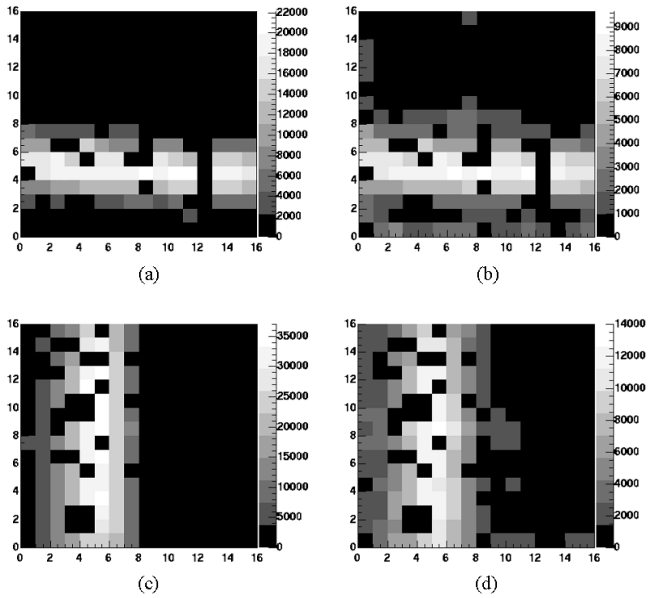

Fig. 11. Images of line sources filled with ^{99m}Tc. Images are taken with (a) the all-purpose collimator in air and (b) with 10 cm scattering block, and (c) the high-sensitivity collimator in air and (d) with 10 cm scattering block. Dark pixels that should have counts in them are dead or noisy pixels that have been turn off in the readout IC. Each module has about 10% to 20% dead or noisy pixels.

TABLE II
SYSTEM SPATIAL RESOLUTION MEASURED WITH THE 16-MODULE CAMERA

	All-Purpose Collimator			High-Sensitivity Collimator		
	In Air	5 cm Block	10 cm Block	In Air	5 cm Block	10 cm Block
FWHM (mm)	8.7	8.8	9.0	11.2	11.1	11.5
FWTM (mm)	15.8	16.0	16.5	20.4	20.3	21.0

VII. References

[1] J. Strobel, N. H. Clinthorne, and W. L. Rogers, "Design studies for a cesium iodide silicon photodiode gamma camera," *J. Nucl. Med.*, vol. 38, pp. 31P, 1997.

[2] G. J. Gruber, W. W. Moses, S. E. Derenzo, N. W. Wang, E. Beuville, and M. H. Ho, "A discrete scintillation camera module using silicon photodiode readout of CsI(Tl) crystals for breast cancer imaging," *IEEE Trans. Nucl. Sci.*, vol. 45, pp. 1063–1068, 1998.

[3] B. E. Patt, J. S. Iwanczyk, C. Rossington Tull, N. W. Wang, M. P. Tornai, and E. J. Hoffman, "High resolution CsI(Tl)/Si-PIN detector development for breast imaging," *IEEE Trans. Nucl. Sci.*, vol. 45, pp. 2126–2131, 1998.

[4] M. P. Tornai, B. E. Patt, J. S. Iwanczyk, C. S. Levin, and E. J. Hoffman, "Discrete scintillator coupled mercuric iodide photodetector arrays for breast imaging," *IEEE Trans. Nucl. Sci.*, vol. 44, pp. 1127–1133, 1997.

[5] Model 2020tc Imager from Digirad Corporation, San Diego, CA 92126-6334 (http://www.digirad.com).

[6] J. F. Butler, C. L. Lingren, S. J. Friesenhahn, F. P. Doty, W. L. Ashburn, R. L. Conwell, et al., "CdZnTe solid-state gamma camera," *IEEE Trans. Nucl. Sci.*, vol. 45, pp. 1158–1165, 1998.

[7] M. Singh and E. Mumcuoglu, "Design of a CZT based BreastSPECT system," *IEEE Trans. Nucl. Sci.*, vol. 45, pp. 1158–1165, 1998.

[8] Y. Eisen, A. Shor, I. Mardor, "CdTe and CdZnTe gamma ray detectors for medical and industrial imaging systems", *Nucl. Instr. Meth.*, vol. A428, pp 158-170, 1999.

[9] K. Blazek, F. de Notaristefani, F. Maly, et al., "YAP multi-crystal gamma camera prototype," *IEEE Trans. Nucl. Sci*, vol. 42, pp. 1474-1482, 1995.

[10] F. de Notaristefani, R. Pani, F. Scopinaro, et al., "First results from a YAP:Ce gamma camera for small animal studies," *IEEE Trans. Nucl. Sci.*, vol. 43, pp. 3264-3271, 1996.

[11] R. Wojcik, B. Kross, D. Steinback, and A. Weisenberger, "High spatial resolution gamma imaging detector based on a 5" diameter Hammatsu PSPMT," *IEEE Trans. Nucl. Sci.*, vol. 45, pp. 487-491, 1997.

[12] R. Pani, A. Soluri, R. Scafe, et al., "Multi-PSPMT scintillation camera," *IEEE Trans. Nucl. Sci*., vol. 46, pp. 702-708, 1999.

[13] M. Williams, A. Goode, V. Galbis-Reig, et al., "Performance of a PSPMT based detector for scintimammogrpahy," *Phys. Med. Biol.*, vol. 45, pp. 781-800, 2000.

[14] S. Majewski, D. Kieper, E. Curran, C. Keppel, B. Kross, A. Palumbo, et al., "Optimization of dedicated scintimammography procedure using detector prototypes and compressible phantoms," *IEEE Trans. Nucl. Sci.*, vol. 48, pp. 822-829, 2001.

[15] G. J. Gruber, W.-S. Choong, W. W. Moses, S. E. Derenzo, S. E. Holland, M. Pedrali-Noy, et al., "A compact 64-pixel CsI(Tl)/Si PIN photodiode imaging module with IC readout," *IEEE Trans. Nucl. Sci.*, vol. 49, pp. 147-152, 2002.

[16] S. E. Holland, N. W. Wang, and W. W. Moses, "Development of low noise, back-side illuminated silicon photodiode arrays," *IEEE Trans. Nucl. Sci.*, vol. 44, pp. 443–447, 1997.

[17] M. Pedrali-Noy, G. J. Gruber, B. Krieger, E. Mandelli, G. Meddeler, W. W. Moses et al., "PETRIC—A Positron Emission Tomography Readout Integrated Circuit," *IEEE Trans. Nucl. Sci.*, vol. 48, pp. 479-484, 2001.

[18] W. W. Moses, E. Beuville, and M. H. Ho, "A "Wiiner-Take-All" IC for determining the crystal of interaction in PET detectors", *IEEE Trans. Nucl. Sci.*, vol. 43, pp. 1615-1618, 1996.

[19] G. J. Gruber, W. W. Moses, and S. E. Derenzo, "Monte Carlo simulation of breast tumor imaging properties with compact, discrete gamma cameras," *IEEE Trans. Nucl. Sci.*, vol. 46, pp. 2119-2123, 1999.

[20] NEMA Standards Publication NU 1-1994: Performance Measurements of Scintillation Cameras, National Electrical Manufacturers Association, Washington, DC, 1994.